# Electronic Supplementary Information

## Interfacial Coupling between Noble Metal Nanoparticles and Metal-Organic Frameworks for Enhanced Catalytic Activity

Yongde Tong,[a,b‡] Guangxin Xue,[a‡] Hui Wang,[a‡] Mei Liu,[a] Jin Wang,[b] Changlong Hao,[a] Xiaofei Zhang,[a] Dawei Wang,[a] Xinghua Shi,[a] Wei Liu,[*b] Guodong Li[*a] and Zhiyong Tang[a]

[a] CAS Key Laboratory of Nanosystem and Hierachical Fabrication, CAS Center for Excellence in Nanoscience, National Center for Nanoscience and Technology, Beijing 100190, P.R. China
E-mail: liguodong@nanoctr.cn

[b] College of Chemistry and Chemical Engineering, University of Chinese Academy of Sciences, Beijing 100049, P.R. China
E-mail: weiliu@ucas.ac.cn

* Corresponding authors.

‡ These authors contributed equally to this work.

**Experimental Section**

**Reagents.** 2-methlimidazole (98%) was purchased from Aladdin. Zinc acetate dehydrate (98%), cobalt(II) nitrate hexahydrate (98%), choloroplatinie acid (Pt ≥ 37.5%) and palladium(II) chloride were bought from Alfa Aesar. Chloroauric acid tetrahydrate (gold contents ≥ 47.8%) was achieved from Sinopharm chemical Reagent Co. Ltd. Hydrochloric acid, methanol and other solvents were bought from Beijing Chemical Works.

**Characterization.** Scanning electron microscopy (SEM) measurement was performed on a Hitachi S4800 scanning electron microscope at 6.0 kV. Transmission electron microscopy (TEM) and high-resolution TEM (HRTEM) imaging were carried out using Tecnai $G^2$ F20 S-TWIN at 200 kV. High angle annular dark field scanning transmission electron microscopy (HAADF-STEM) imaging and energy-dispersive X-ray spectroscopy (EDS) elemental mapping were carried out on JEM-ARM 200F at 200 kV. Powder X-ray diffraction (XRD) was performed on D/max-TT/max-TTRIII at a scanning rate of 4 ° $min^{-1}$ to identify the crystallographic phase of the samples. X-ray photoelectron spectroscopy (XPS) was used to analyze the chemical states of the atoms on the sample surface, as performed on a Thermo Scientific Escalab 250Xi. The XPS data were calibrated using the binding energy of C 1*s* (284.6 eV) as standard. Metal loading amounts were tested by Perkin Elmer NexION 300X ICP Mass Spectrometer.

**Synthesis of ZIF-67(Co).** According to the literature,[1] ZIF-67 was synthesized using colloid chemical method. A mixture solution of 2-methylimidazole (6.489 g, 79.0 mmol) and methanol (200 mL) was rapidly poured into a solution of $Co(NO_3)_2 \cdot 6H_2O$ (2.933 g, 10.0 mmol) in 200 mL methanol under stirring for 6 h. The mixture turned into purple colour instantaneously and turbid slowly, and then the products were separated from the milky dispersion by centrifugation at 8000 rpm. Subsequently, the precipitates were washed with fresh methanol for three times. The products were dried at 80°C in air for 6 h.

**Synthesis of ZIF-8(Zn).** According to the literature,[2] 350 mg $Zn(CH_3COOH)_2$ and 540 mg 2-methylimidazole were poured into a flask together, followed by adding 80 mL methanol into the mixture solution. The solution was stirred at room temperature for 5 min, and then aged for 24 h.The products were separated from the milky dispersion by centrifugation at 8000 rpm, and washed with fresh methanol for three times. The products were dried at 80°C in air for 6 h.

**Synthesis of ZIF-67(Co)@M (M = Pd, Pt or Au).** According to the literature,[3] 20 mg ZIF-67(Co) was dispersed in 10 mL methanol by ultrasonic treatment for 10 min. Afterwards, 300 μL $H_2PdCl_4$ aqueous solution (50 mM) was added into the ZIF solution drop by drop under stirring for 6 h at room temperature. After that, 1mL methanol containing 7.2 mg $NaBH_4$ was added into the system to reduce the precursors for 1 h. Subsequently, the obtained ZIF-67@Pd samples were separated from the turbid liquid by centrifugation at 8000 rpm, followed by washing with fresh methanol. Finally, the products were dried in vacuum at room temperature for 12 h. Similarly, 300 μL $H_2PdCl_4$ aqueous solution (50 mM) was replaced by 300 μL $H_2PtCl_4$ aqueous solution (50 mM) or 300 μL $HAuCl_4$ aqueous solution (50 mM) to achieve the ZIF-67(Co)@Pt or ZIF-67(Co)@Au samples.

**Synthesis of ZIF-8(Zn)@M (M = Pd, Pt or Au).** 20 mg ZIF-8(Zn) was dispersed in 10 mL methanol by ultrasonic treatment for 10 min. Afterwards, 300 μL $H_2PdCl_4$ aqueous solution (50 mM) was added into the ZIF solution drop by drop under stirring for 6 h at room temperature. After that, 1 mL methanol containing 7.2 mg $NaBH_4$ was added into the system to reduce the precursors for 1 h. Subsequently, the obtainedZIF-8@Pd samples were separated from the turbid liquid by centrifugation at 8000 rpm, followed by washing with fresh methanol. Finally, the products were dried in vacuum at room temperature for 12 h. Similarly, 300 μL $H_2PdCl_4$ aqueous solution (50 mM) was replaced by 300 μL $H_2PtCl_4$ aqueous solution (50 mM) or 300 μL $HAuCl_4$ aqueous solution (50 mM) to achieve the ZIF-8(Zn)@Pt or ZIF-8(Zn)@Au samples.

**Synthesis of Pd, Pt and Au.** 35.9 mg $NaBH_4$ was mixed with 5 mL methanol triplicated by ultrasonic dissolution, followed by dropping the $NaBH_4$ solution into 3 mL $H_2PdCl_4$ ($H_2PtCl_4$, or $HAuCl_4$) aqueous solution (50 mM) slowly under stirring, respectively. And then, the mixture was stirred at room temperature for 1 h. Subsequently, the obtained Pd (Pt or Au) were separated from the turbid liquid by centrifugation at 8000 rpm, followed by washing with pure water for twice. Finally, the products were dried in vacuum at room temperature for 6 h, which were used for XPS measurements.

**Synthesis of ZIF-8(Zn) derived carbon materials.**[3] ZIF-8(Zn) powders (200 mg) were directly heat-treated under nitrogen flow to remove the impurity of Zn. The temperature was increased to 800$^{o}$C with a heating rate of 5$^{o}$C min$^{-1}$, and the powders were annealed at 800$^{o}$C for 5 h. After that, the obtained samples were washed extensively by HCl solution (35 wt%)

to remove residual Zn component. Energy-dispersive X-ray spectroscopy (EDX) measurement verified that there was only less than 0.4 wt% of Zn left in the final products.

**Synthesis of C(carbon)@M (M = Pd, Pt, Au).** 20 mg C(carbon) was dispersed in 10 mL methanol by ultrasonic treatment for 10 min. Afterwards, 300 μL $H_2PdCl_4$ aqueous solution (50 mM) was added into the C(carbon) solution drop by drop under stirring for 6 h at room temperature. After that, 1 mL methanol containing 7.2 mg $NaBH_4$ was added into the system to reduce the precursors for 1 h. Subsequently, the obtained C(carbon)@Pd samples were separated from the turbid liquid by centrifugation at 8000 rpm, followed by washing with fresh methanol. Finally, the products were dried in vacuum at room temperature for 12 h. Similarly, 300 μL $H_2PdCl_4$ aqueous solution (50 mM) was replaced by 300 μL $H_2PtCl_4$ aqueous solution (50 mM) or 300 μL $HAuCl_4$ aqueous solution (50 mM) to achieve the C(carbon)@Pt or C(carbon)@Au samples.

**Synthesis of ZIF-67(Co)@Pd with Pd sizes of 4.6 and 5.8 nm.** According to the literature,[3] 20 mg ZIF-67(Co) was dispersed in 10 mL methanol by ultrasonic treatment for 10 min. Afterwards, 300 μL $H_2PdCl_4$ aqueous solution (50 mM) was added into the ZIF solution drop by drop under stirring for 6 h at room temperature. After that, 1 mL methanol containing 15 mg and 20 mg $NaBH_4$ was added into the system to reduce the precursors for 1 h, respectively. Subsequently, the obtained ZIF-67@Pd samples were separated from the turbid liquid by centrifugation at 8000 rpm, followed by washing with fresh methanol. Finally, the products with different Pd sizse of 4.6 and 5.8 nm were dried in vacuum at room temperature for 12 h, respectively.

**Catalytic CO oxidation.** Catalytic tests were performed in a continuous flow fixed bed reactor. A quartz tube with an inner diameter of 4 mm was used as the reactor. 40 mg ZIFs(Co/Zn)@M catalysts were mixed with quartz sand in the reactor without any pre-activation. A mini-tube furnace was used for controlling programmed heating. The reaction gas mixture consisting of CO (2 vol%), $O_2$ (16 vol%) and Ar (82 vol%) was passed through the catalyst bed at a total flow rate of 57.5 mL $min^{-1}$, corresponding to a gas hourly space velocity (GHSV) of 86250 mL $h^{-1}$ $g^{-1}_{cat}$. The rate of heating was controlled at 5°C $min^{-1}$. The composition of the influent and effluent gases was determined using an online GC-9860 gas chromatograph equipped with a thermal conductivity detector. The weight of C(carbon)@M catalysts used was listed in Table S2.

**Catalytic liquid-phase benzaldehyde oxidation.** Catalytic oxidation of benzaldehyde was performed in a 100 mL three-necked flask with condenser. The prepared ZIFs(Co/Zn)@M catalysts (10 mg) and acetonitrile (18 mL) were placed in the reactor and sonicated for 10 min. And then, benzaldehyde (2 mL) was added under magnetic stirring. The $O_2$ with a flow rate of 40 mL $min^{-1}$ was introduced on the surface of liquid phase under atmospheric pressure to start the reaction and the reaction temperature was maintained at 25°C. The analysis of the catalytic products was carried out using a gas chromatography equipped with FID detector. Correspondingly, the weight of C(carbon)@M catalysts used was one quarter of that listed in Table S2.

**Theoretical calculation.** To make the computation affordable, the implified structural unit (ZIFs) with methyl replaced by H (as shown in Figure S17) was chosen to study its interaction with the M (M = Pd, Pt and Au) NPs. On the basis of experimental observations, a (4 × 4 × 1) supercell with a three-layered periodic slab separated by a vacuum region of 15 Å was used to model the M(111) surface and its interaction with ZIFs. The bottom layer was fixed and the two upper ones were allowed to relax for M(111) before and after its interaction with ZIFs (ZIFs-M(111)) except for ZIFs-Pt(111), in which only the top layer was allowed to relax to avoid the slipping of layers.

All density-functional theory (DFT) calculations were carried out using Vienna ab initio simulation package (VASP) with plane-wave pseudopotential method.[4,5] The electronic exchange and correlation effects were described by the Perdew-Burke-Ernzerhof (PBE) functional[6] with the generalized gradient approximation (GGA) and the core electrons were described by the full-potential projector augmented wave (PAW) method.[7,8] An energy cutoff of 400 eV for the plane-wave expansion was used and the force on the relaxed atoms was less than -0.03 eV/Å. The spin-polarization was taken into accounted in all calculations. Integrations in the Brillouin zone were performed using a k-point grid generated with the Monkhorst-Pack grid, centered at the Γ-point.

The adsorption energy of CO, $E_{ads}$, was defined as:

$$E_{ads} = E_{surf-gas} - E_{surf} - E_{gas}$$

Where $E_{surf\text{-}gas}$, $E_{surf}$ and $E_{gas}$ were the total energy of slab with CO adsorption, M(111) surface and free CO, respectively.

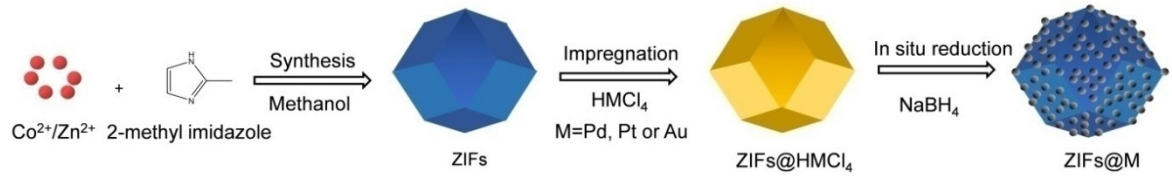


**Fig. S1** Synthesis route for ZIFs(Co/Zn)@M.

In brief, ZIFs with different metal nodes including Co or Zn were firstly prepared by the previously-reported solvothermal methods, known as ZIF-67(Co) or ZIF-8(Zn). Both of the products are uniform icosahedra with mean diameter of 379 and 349 nm (Figs S2 and S3), respectively, and share the identical crystal parameters (Fig. S4). Subsequently, ZIFs were impregnated with inorganic metal precursors including $H_2PdCl_4$, $H_2PtCl_6$ or $HAuCl_4$, respectively, to form homogeneous solutions. Finally, reducing agent $NaBH_4$ was added into the above solutions drop by drop to form the ZIFs(Co/Zn)@M catalysts including ZIF-67(Co)@M and ZIF-8(Zn)@M (M = Pd, Pt or Au).

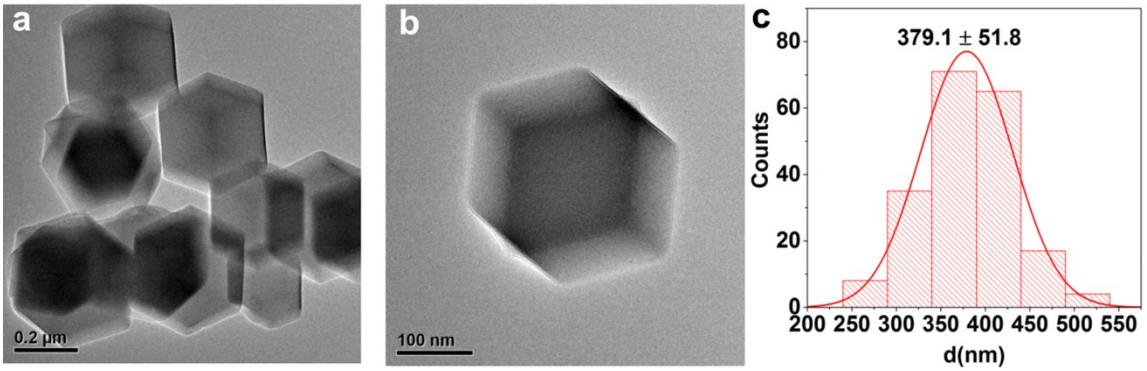


**Fig. S2** (a) Large-scale and (b) magnified TEM images of ZIF-67(Co), and (c) corresponding size histogram of ZIF-67(Co).

The obtained ZIF-67(Co) samples are uniform icosahedra with average diameter of 379 nm.

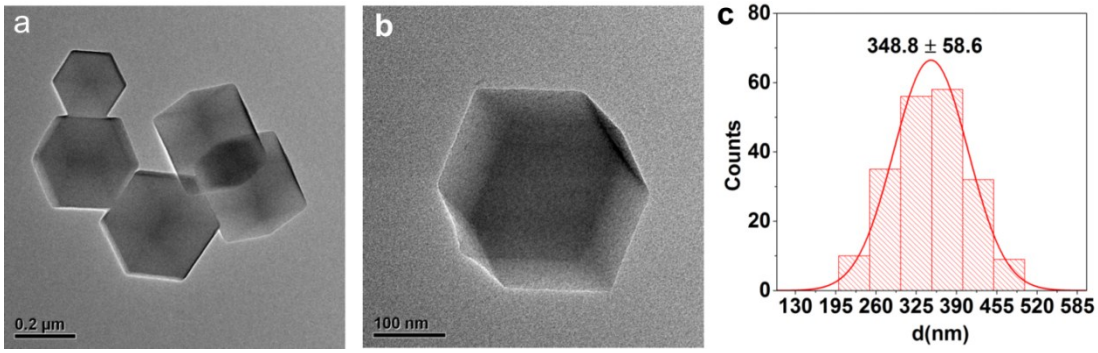


**Fig. S3** (a) Large-scale and (b) magnified TEM images of ZIF-8(Zn), and (c) corresponding size histogram of ZIF-8(Zn).

The obtained ZIF-8(Zn) samples are uniform icosahedra with mean diameter of 349 nm.

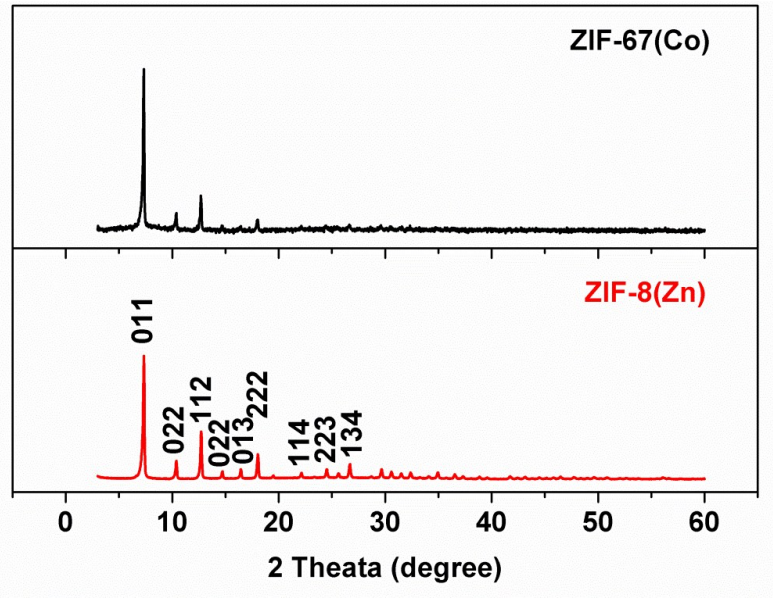


**Fig. S4** XRD patterns of ZIF-67(Co) and ZIF-8(Zn).

Both ZIF-67(Co) and ZIF-8(Zn) share the same cubic phase and have the identical crystal parameters.

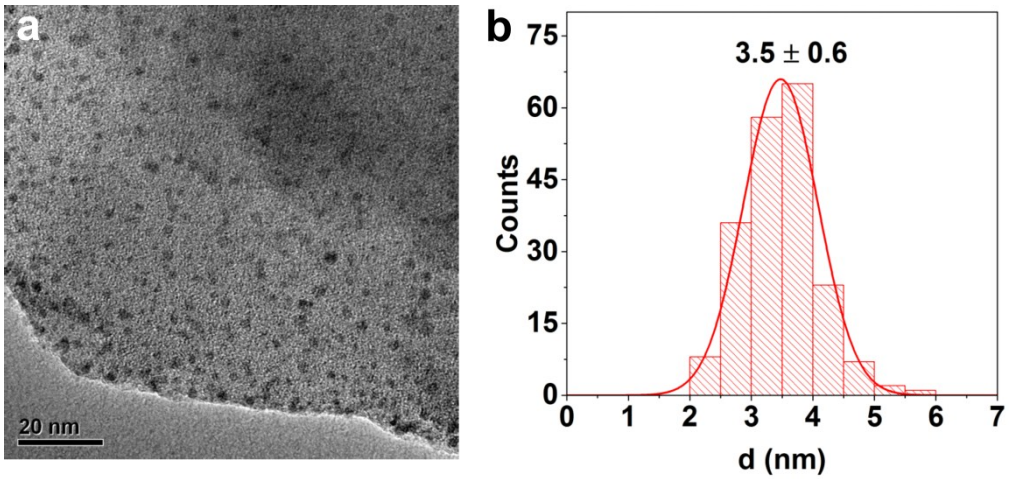


**Fig. S5** (a) TEM image of ZIF-67(Co)@Pd and (b) corresponding size histogram of Pd NPs shown in (a).

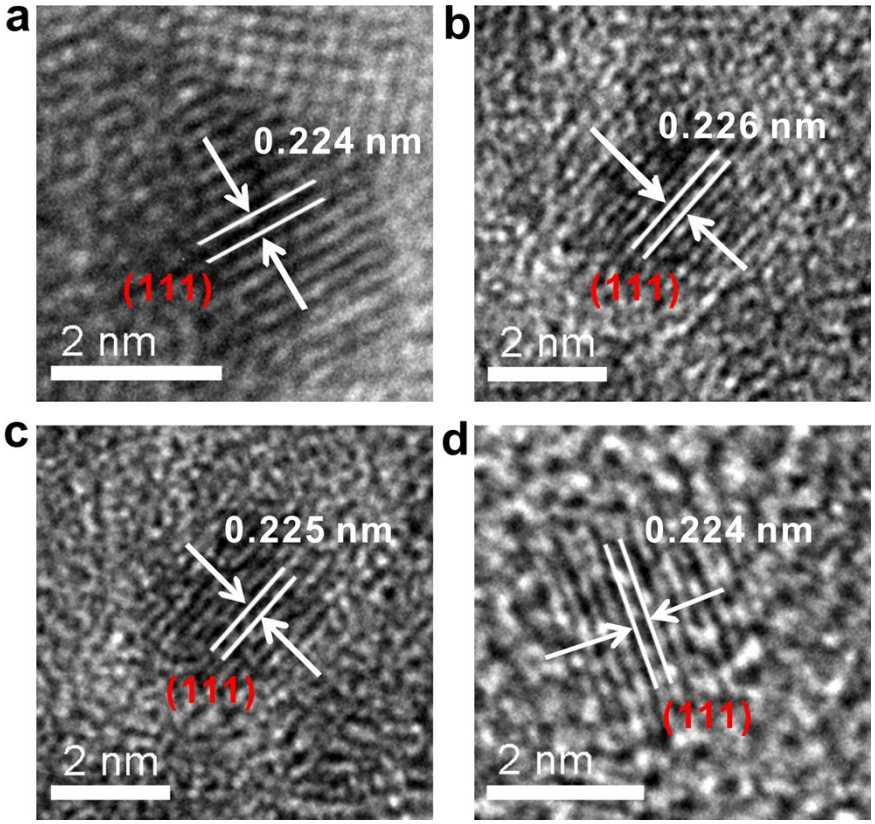


**Fig. S6** (a-d) HR-TEM images of Pd NPs on ZIF-67(Co)@Pd samples.

It is noticed that all the Pd NPs on ZIF-67(Co)@Pd samples mainly expose the (111) facets.

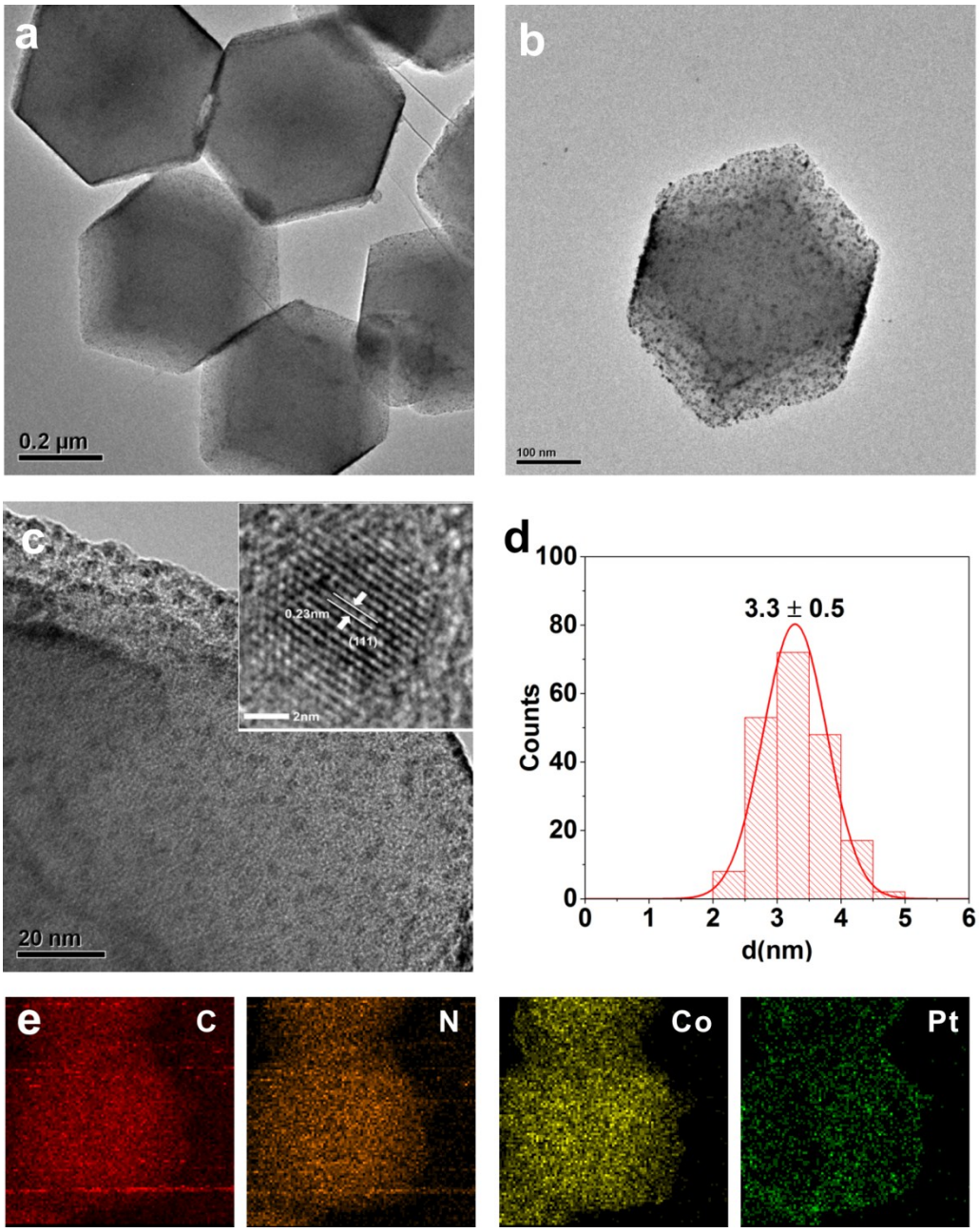


**Fig. S7** (a) Large-scale TEM image of ZIF-67(Co)@Pt. (b) TEM image of single ZIF-67(Co)@Pt. (c) Magnified TEM image of ZIF-67(Co)@Pt. Inset: HRTEM image of Pt NP. (d) Size histogram of Pt NPs in (c). (e) HAADF-STEM elemental mapping of single ZIF-67(Co)@Pt.

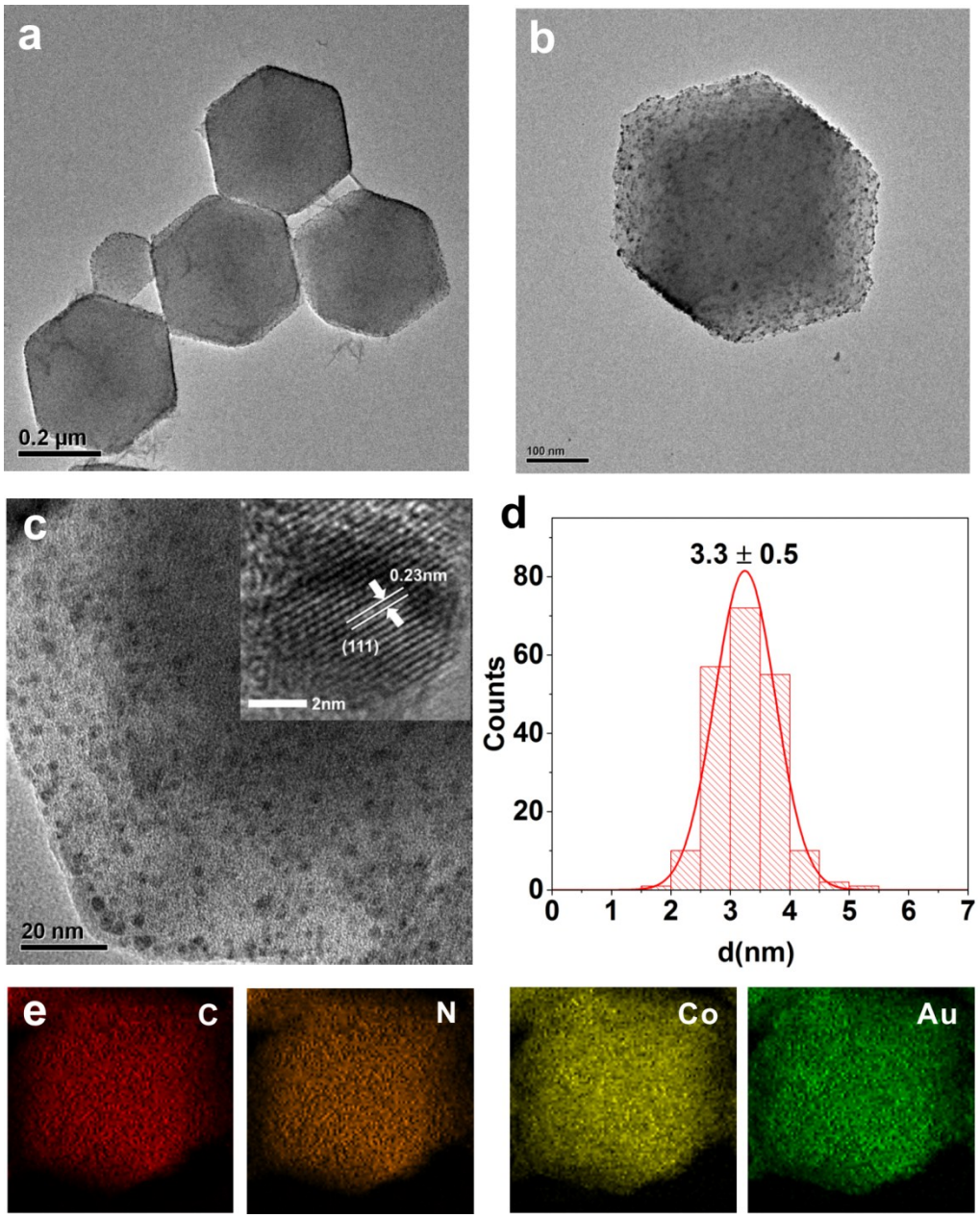


**Fig. S8** (a) Large-scale TEM image of ZIF-67(Co)@Au. (b) TEM image of single ZIF-67(Co)@Au. (c) Magnified TEM image of ZIF-67(Co)@Au. Inset: HRTEM image of Au NP. (d) Size histogram of Au NPs in (c). (e) HAADF-STEM elemental mapping of single ZIF-67(Co)@Au.

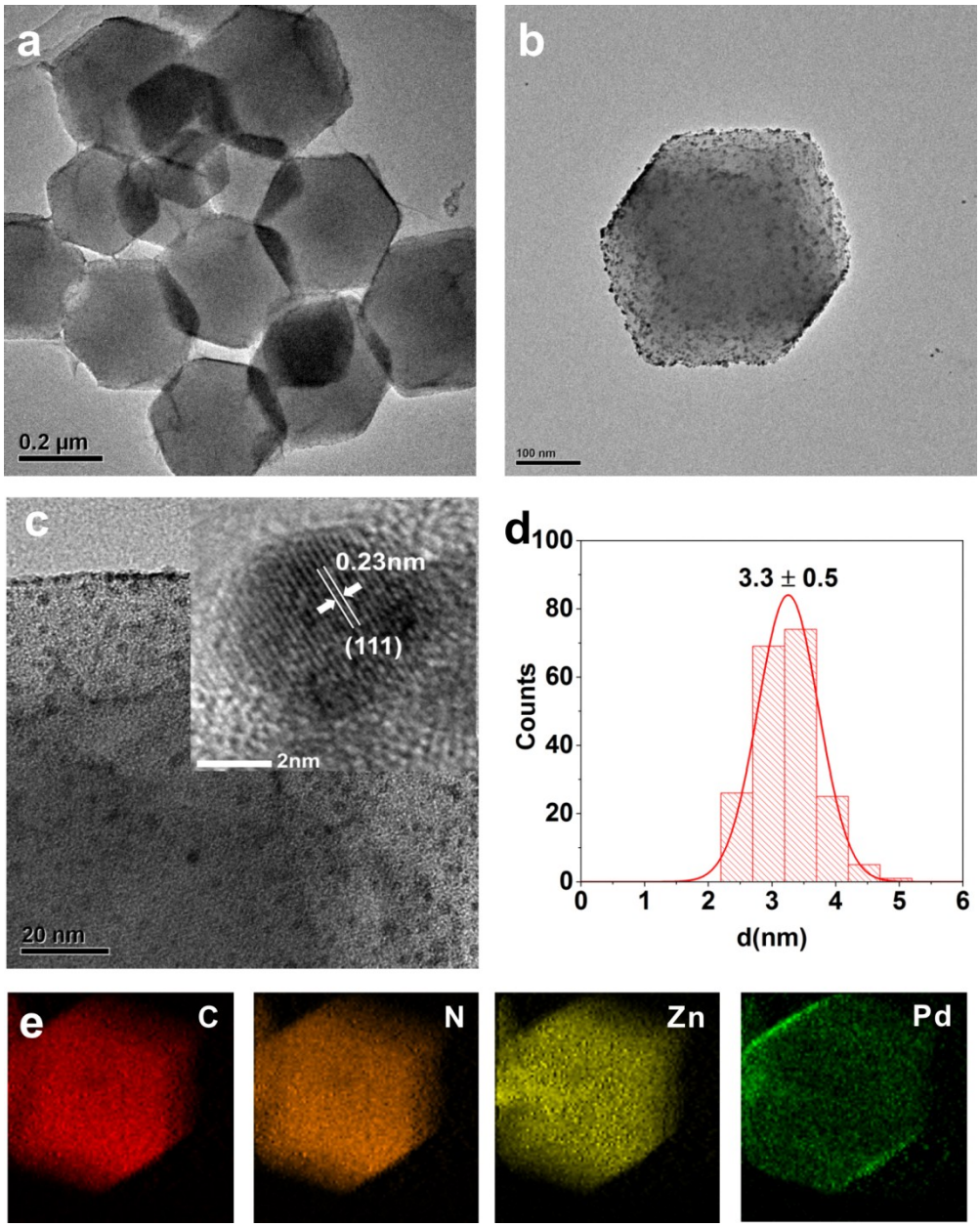


**Fig. S9** (a) Large-scale TEM image of ZIF-8(Zn)@Pd. (b) TEM image of single ZIF-8(Zn)@Pd. (c) Magnified TEM image of ZIF-8(Zn)@Pd. Inset: HRTEM image of Pd NP. (d) Size histogram of Pd NPs in (c). (e) HAADF-STEM elemental mapping of single ZIF-8(Zn)@Pd.

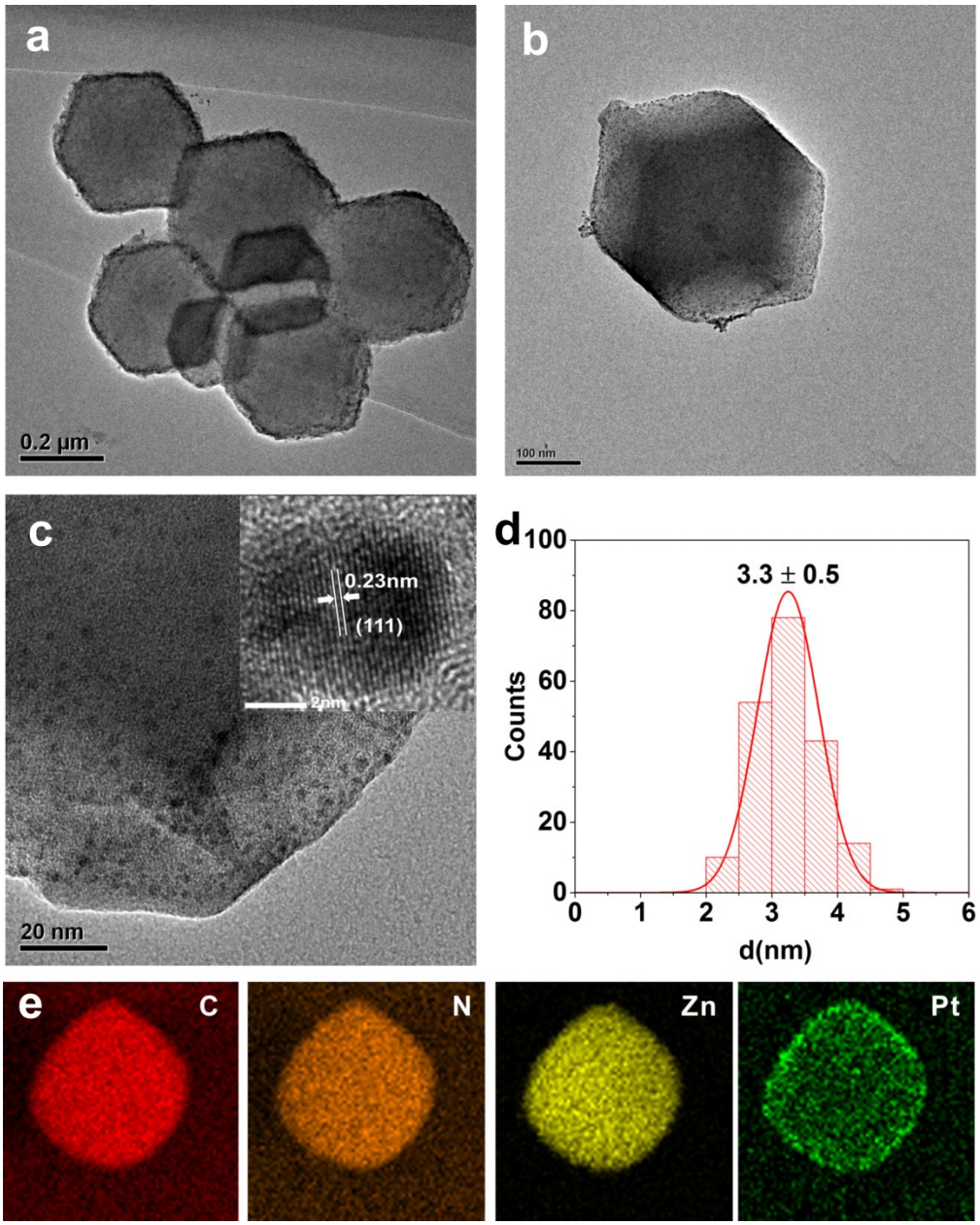


**Fig. S10** (a) Large-scale TEM image of ZIF-8(Zn)@Pt. (b) TEM image of single ZIF-8(Zn)@Pt. (c) Magnified TEM image of ZIF-8(Zn)@Pt. Inset: HRTEM image of Pt NP. (d) Size histogram of Pt NPs in (c). (e) HAADF-STEM elemental mapping of single ZIF-8(Zn)@Pt.

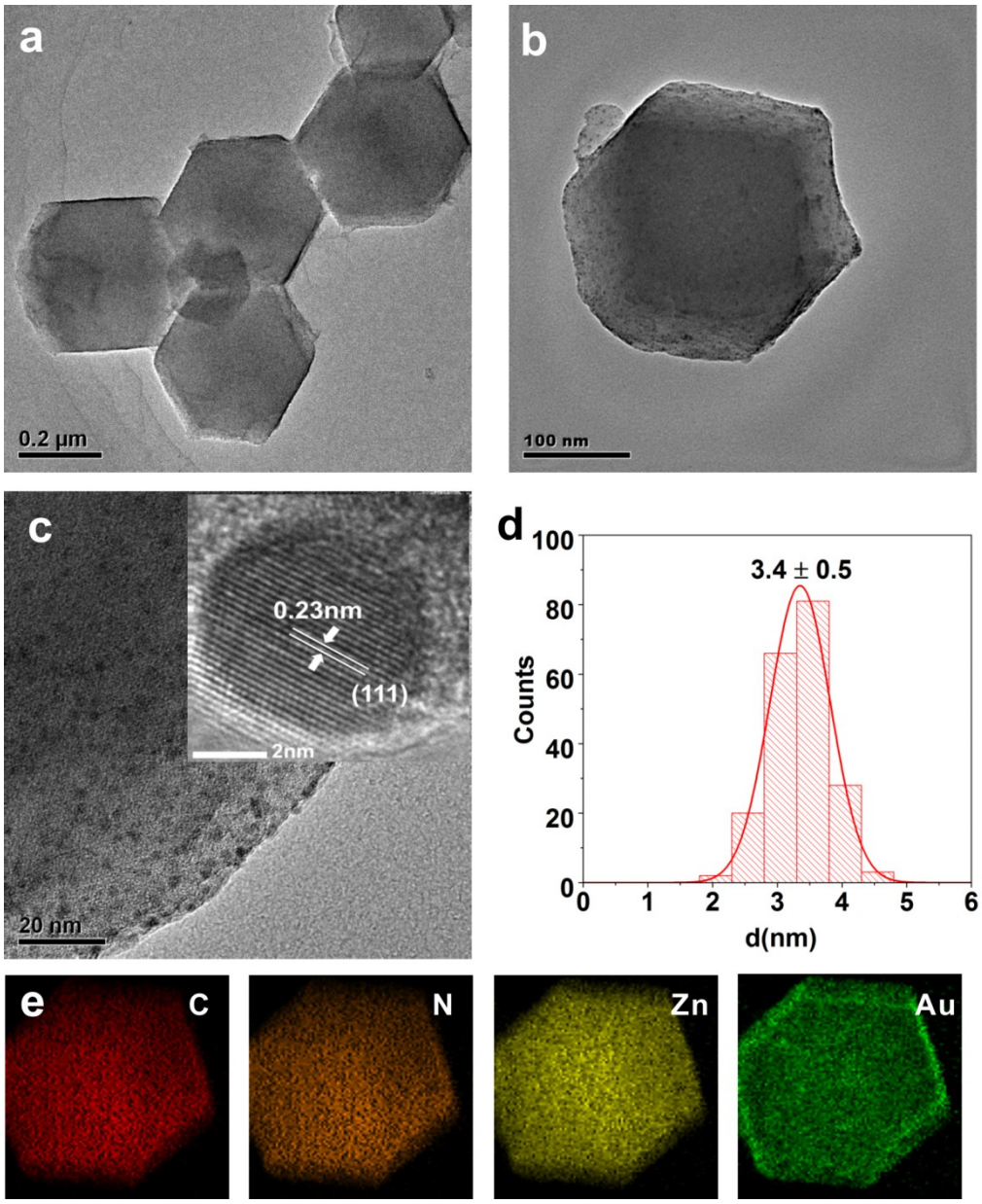


**Fig. S11** (a) Large-scale TEM image of ZIF-8(Zn)@Au. (b) TEM image of single ZIF-8(Zn)@Au. (c) Magnified TEM image of ZIF-8(Zn)@Au. Inset: HRTEM image of Au NP. (d) Size histogram of Au NPs in (c). (e) HAADF-STEM elemental mapping of single ZIF-8(Zn)@Au.

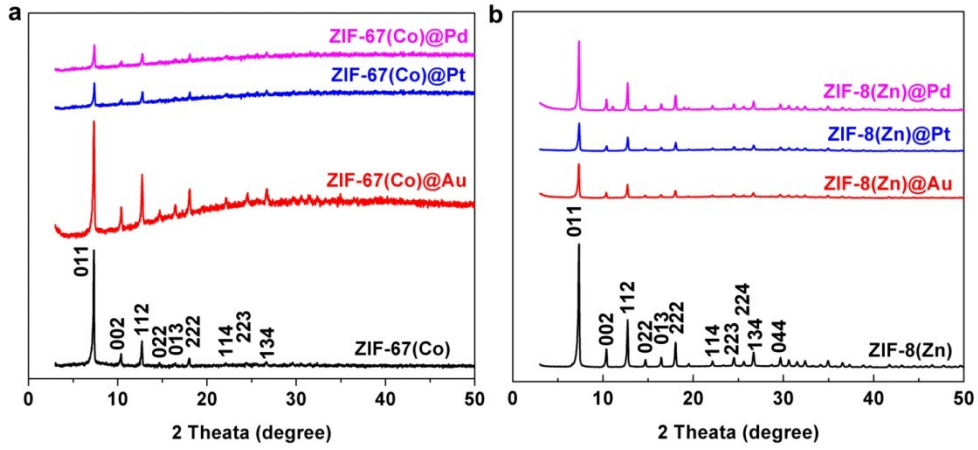


**Fig. S12** XRD patterns of (a) ZIF-67(Co)@M (M = Pd, Pt or Au) and pure ZIF(Co)-67, and (b) ZIF-8(Zn)@M and pure ZIF-8(Zn).

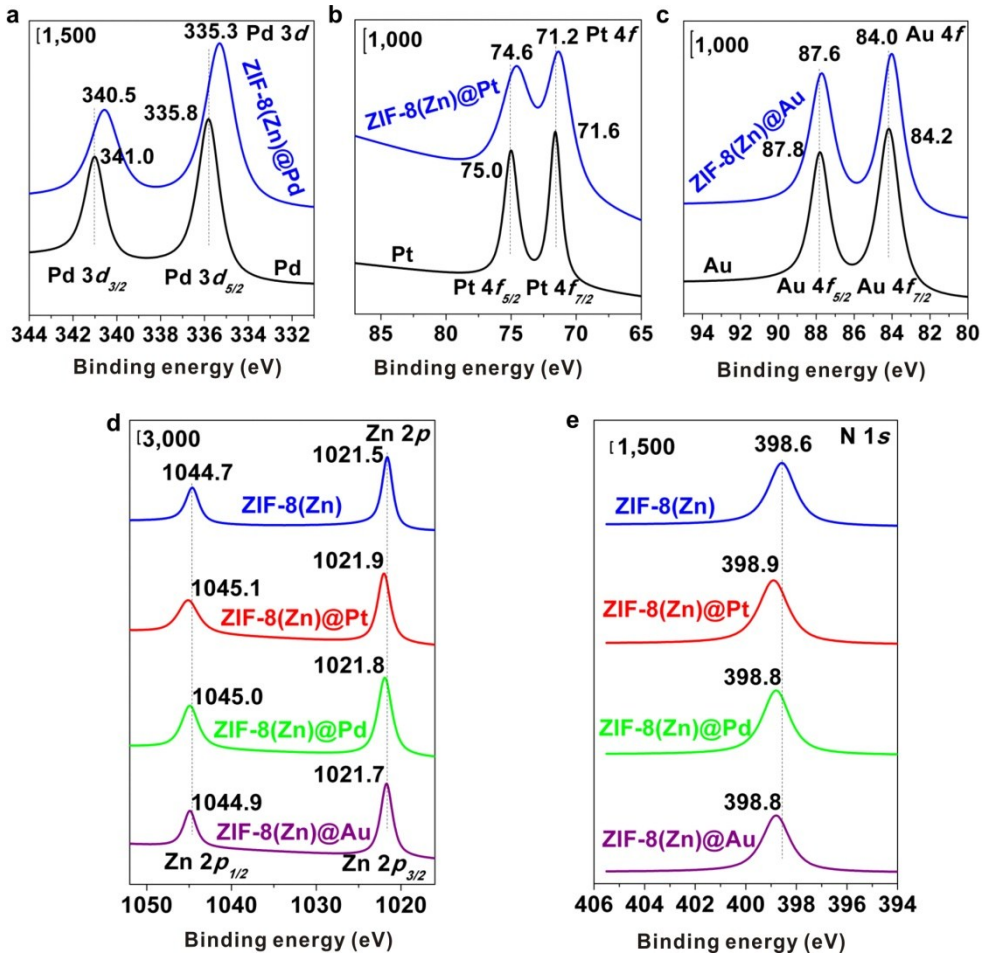


**Fig. S13** XPS profiles of different ZIF-8(Zn)@M catalysts in respect with pure ZIF-8(Zn), Pd NPs, Pt NPs and Au NPs. (a) Pd 3*d* level, (b) Pt 4*f* level, (c) Au 4*f* level, (d) Zn 2*p* level, (e) N 1*s* level. Numbers adjacent to dashed lines represent the binding energy values of the corresponding peaks.

XPS spectra corresponding to Pd 3*d*, Zn 2*p* and N 1*s* core levels of the supported ZIF-8(Zn)@Pd are investigated along with pure Pd NPs and ZIF-8(Zn) samples (Fig. S13a, d and e). The Pd $3d_{5/2}$ binding energy for pure Pd NPs is 335.8 eV, which is assigned to zero-valent Pd in the metallic state.[9] As for ZIF-8(Zn)@Pd, Pd $3d_{5/2}$ binding energy shifts toward a lower value of 335.3 eV whereas the corresponding binding energy of Zn $2p_{3/2}$ and N 1*s* shifts to higher values of 1021.8 and 398.8 eV, compared with 1021.5 eV assigned to Zn (II) and 398.6 eV assigned to N species for pure ZIF-8(Zn). In addition, the analogous binding energy shifts for Pt $4f_{7/2}$ and Au $4f_{7/2}$ as well as Zn $2p_{3/2}$ and N 1*s* are also observed in the supported ZIF-8@Pt and ZIF-8@Au (Fig. S13b, c, d and e).

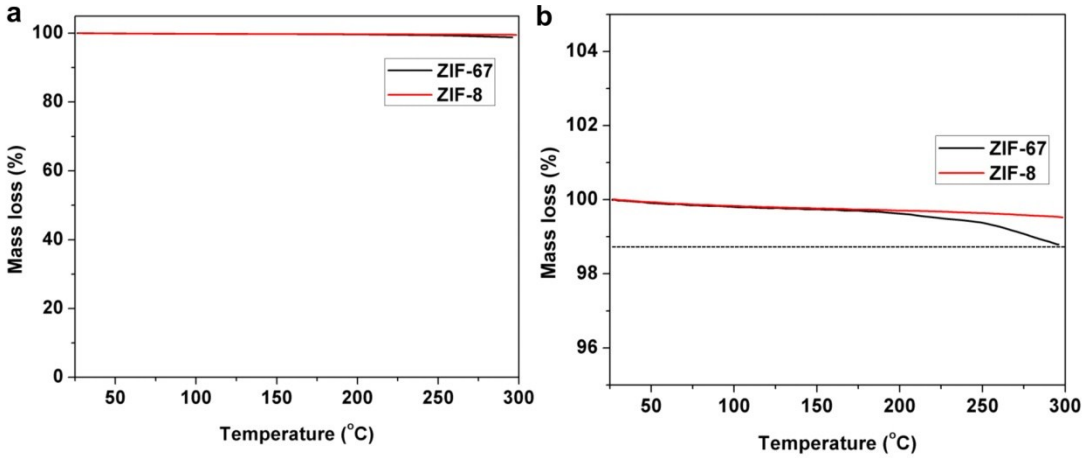


**Fig. S14** TG data for the thermal stability of pure ZIF-8(Zn) and ZIF-67(Co) under the air atmosphere ($N_2$ and $O_2$ mixture).

Before the test, the ZIF-8(Zn) and ZIF-67(Co) samples are subjected to heat treatment at 100°C for 30 min to dry them, and then the mass loss behaviors are tested by increasing the reaction temperature from 25 to 300°C at a heating rate of 5°C/min. The results indicate that no obvious mass loss (less than 1.2%) is observed at the same reaction temperature range of Fig. 3, suggesting that almost no decomposition and solvent loss occur and the CO observed during the catalytic process is only from the original reactant gas.

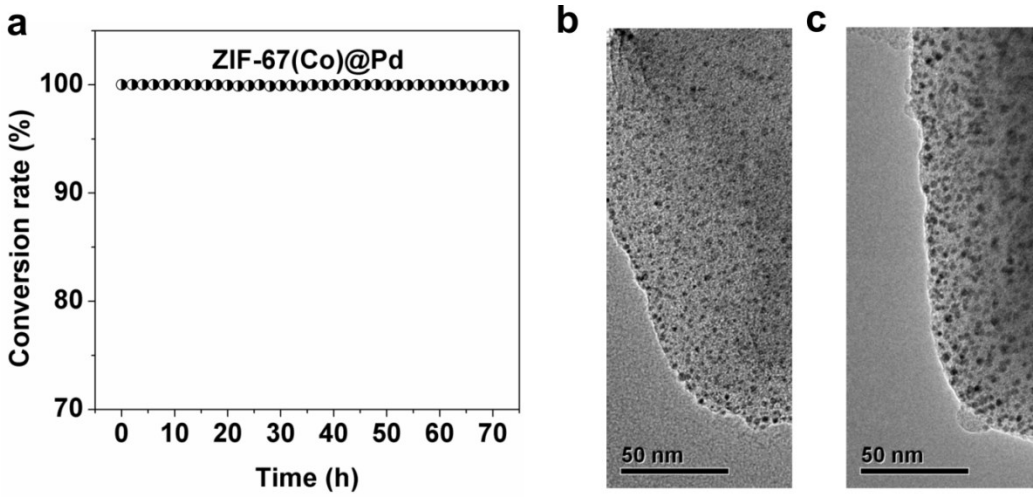


**Fig. S15** (a) Stability test of ZIF-67(Co)@Pd, and corresponding morphology of catalyst (b) before and (c) after catalytic reaction.

Evidently, ZIF-67(Co)@Pd exhibits excellent catalytic stability over 72 h reaction without any activity decay (Fig. S15a), likely due to presence of the strong interfacial interaction between Pd NPs and ZIF-67(Co) (Fig. 2). Such a high stability is also verified by TEM survey (Fig. S15b and c), where no evident morphological difference between fresh and used catalysts is observed.

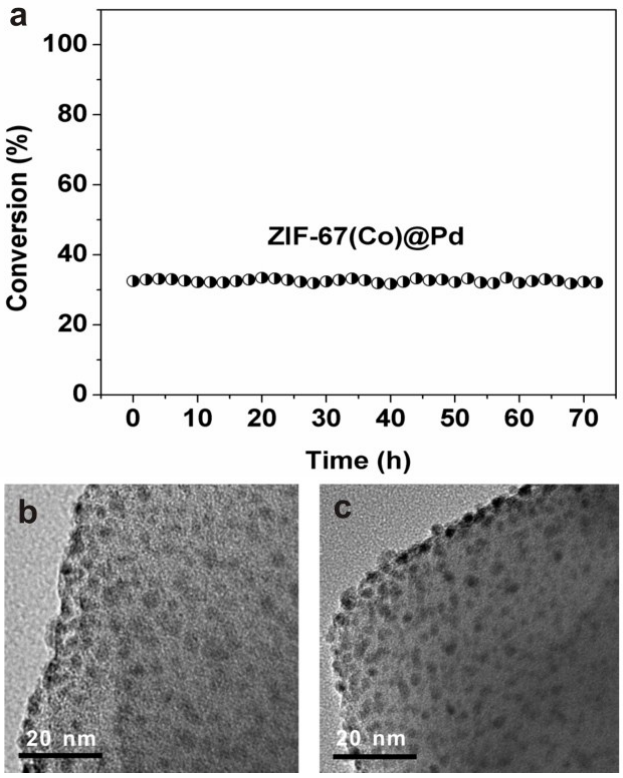


**Fig. S16** (a) Stability test of ZIF-67(Co)@Pd sample when the CO conversion rate is about 33% at the reaction temperature of 80°C, and corresponding morphology of catalyst (b) before and (c) after catalytic reaction.

When the reaction temperature is up to 80°C, ZIF-67(Co)@Pd exhibits excellent catalytic activity of around 33%. At this reaction condition, ZIF-67(Co)@Pd exhibits excellent catalytic stability over 72 h reaction without any activity decay (Fig. S16a). Such a high stability is also verified by TEM survey (Fig. S16b and c), where no evident morphological difference between fresh and used catalysts is observed.

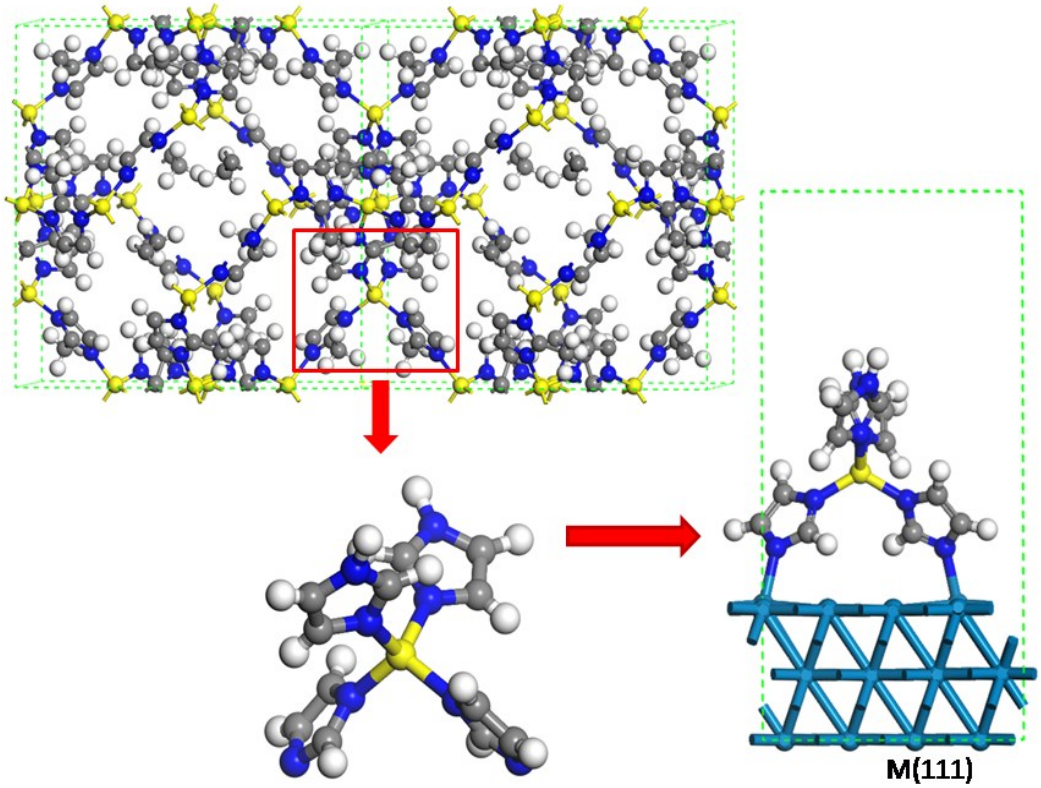


**Fig. S17** Structure of ZIFs(Co/Zn), and model of the interaction between ZIFs(Co/Zn) and M(111) planes (M = Pd, Pt and Au). Colour scheme: H(white), N (blue), C(grey), and Zn/Co (yellow).

On the basis of experimental observation, a (4×4×1) super cell with a three-layered periodic slab separated by a vacuum region of 15 Å was used to model the M(111) surface and its interaction with ZIFs. The lowest layer was fixed and the two upper ones were allowed to relax in all the calculations. All density-functional theory (DFT) calculations were carried out using Vienna ab initio simulation package (VASP) with plane-wave pseudo potential method.[4,5]

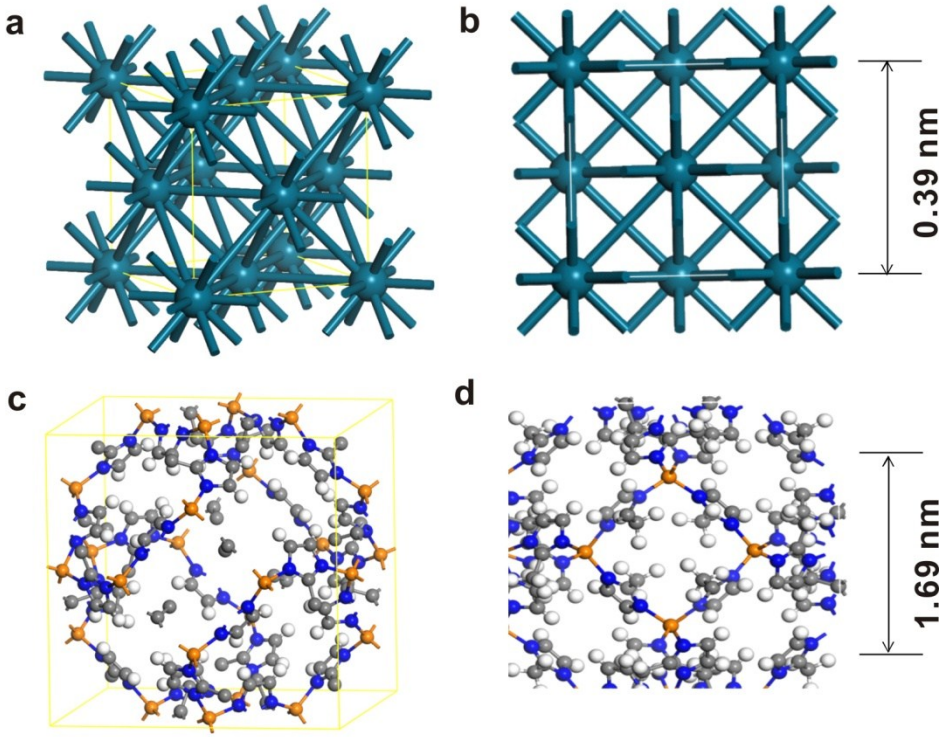


**Fig. S18** Spatial coordination and distribution of different elements in individual unit. (a, b) Pd atom arrangement in the crystal structure from different views. (c, d) Zn/Co, C, N and H atom arrangement in the crystal structure from different views. Colour scheme: H (white), N (blue), C (grey), Zn/Co (orange), and Pd (light blue).

Using ZIF-67(Co)@Pd as the representative, in a cubic Pd unit (0.39 × 0.39 $nm^2$), four atoms are located at the corner and one atom is at the center (Fig. S18a and b), corresponding to each Pd atom in one unit cell (4*1/8 + 1*1/2, Fig. S18b). Similarly, as shown in Fig. S18c and d, four Co atoms are located on the surface of the cubic ZIF unit, corresponding to two Co atoms in one unit cell (4*1/2). Furthermore, the surface area of a cubic Pd unit and a ZIF-67(Co) unit is 0.1521 $nm^2$ and 2.8561 $nm^2$. Based on the above structural analysis, it is easily concluded that if Pd NPs are surround by ZIFs, the ratio of Pd to Co atoms at the interfaces should be ~10 [(2.8561/2)/(0.1521/1)]. So, the subsequent density of states for metal NPs and Co/Zn nodes in ZIFs are calculated based on this estimation (Figs S19 and S20).

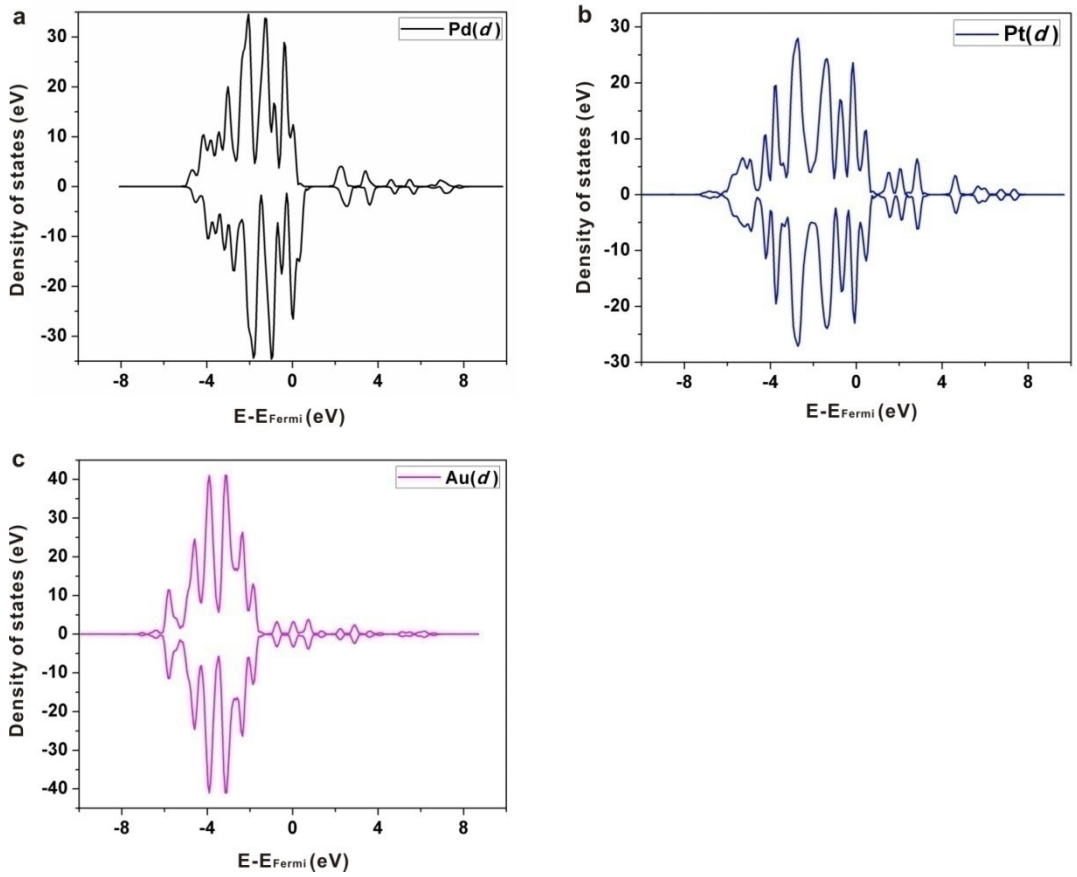


**Fig. S19** Projected density of states (DOSs) for M(111): (a) Pd, (b) Pt, and (c) Au.

The *d*-band center of M(111) locates below Fermi level and follows the order: Pd (-1.43 eV) > Pt (-1.70 eV) > Au (-3.22 eV) (Fig. S19), in good agreement with the general order of their catalytic activity. This calculation result is also supported by many experimental and theoretical works[10-13] that the energy of *d*-bond center is the electronic origin of different adsorption and catalytic activity.

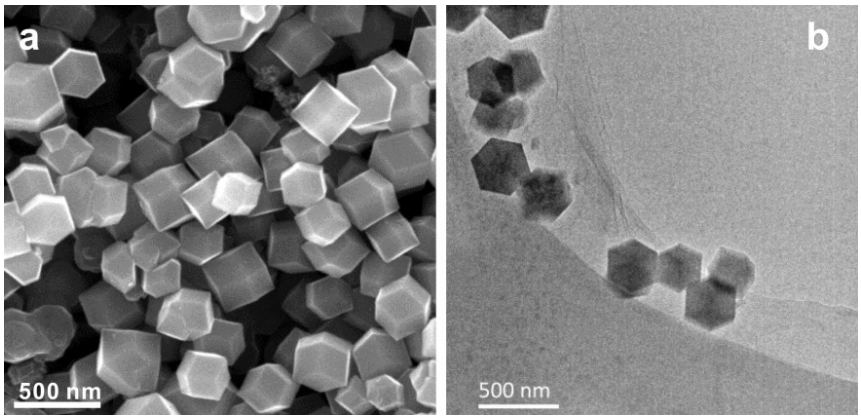


**Fig. S20** (a) SEM and (b) TEM images of ZIF-8(Zn) derived carbon materials.

It is clear that after calcination in inert gas, the obtained carbon materials have almost the same morphology with ZIF-8(Zn) before calcination. Energy-dispersive X-ray spectroscopy (EDX) measurement further shows that there is only less than 0.4 wt% of Zn left in the final products (Fig. S21).

a

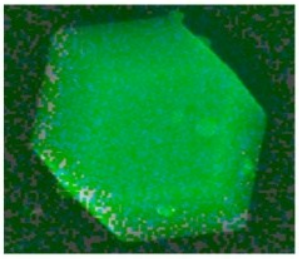

| Element | Content (wt%) |
|---|---|
| C | 46.66 |
| N | 33.13 |
| Zn | 20.20 |
| Total | 100.00 |

b

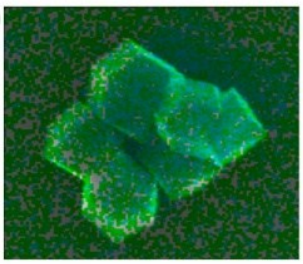

| Element | Content (wt%) |
|---|---|
| C | 89.24 |
| N | 10.38 |
| Zn | 0.38 |
| Total | 100.00 |

**Fig. S21** Energy-dispersive X-ray spectroscopy (EDX) measurements of ZIF-8(Zn) (a) before and (b) after calcination.

EDX measurement indicates that there is only less than 0.4 wt% of Zn left in the final products after calcination.

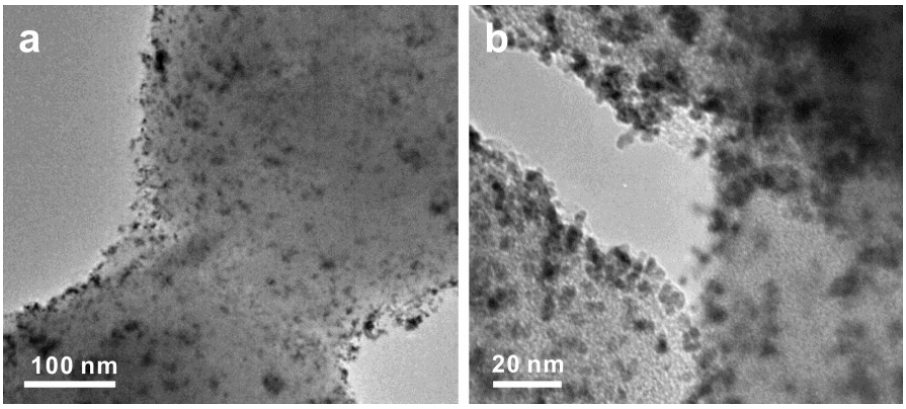


**Fig. S22** TEM images of supported C(carbon)@Pd samples.

As shown in Fig. S22, Pd NPs of ~3 nm in diameter are uniformly dispersed on the surface of C(carbon) supports.

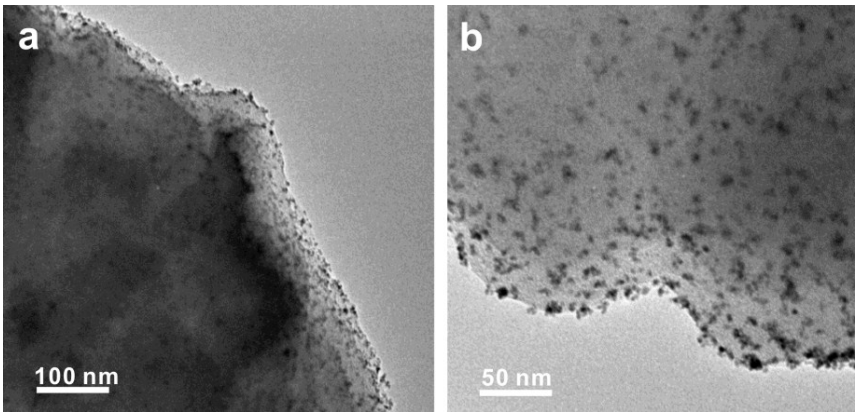


**Fig. S23** TEM images of supported C(carbon)@Pt samples.

As shown in Fig. S23, Pt NPs of ~4 nm in diameter are uniformly dispersed on the surface of C(carbon) support.

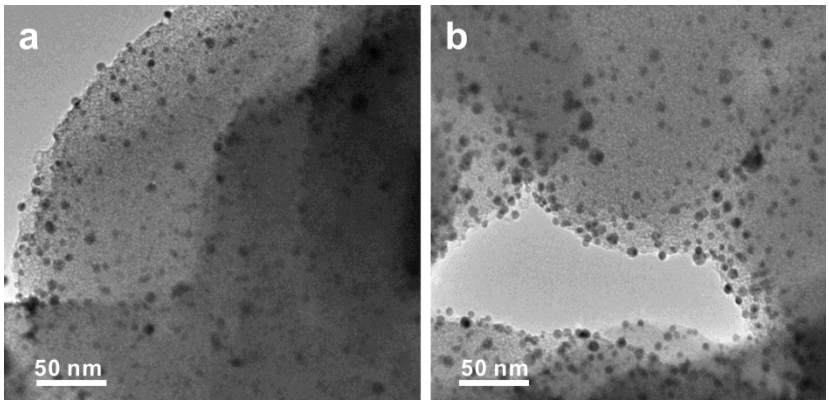


**Fig. S24** TEM images of supported C(carbon)@Au samples.

As shown in Fig. S24, Au NPs of ~5 nm in diameter are uniformly dispersed on the surface of C(carbon) support.

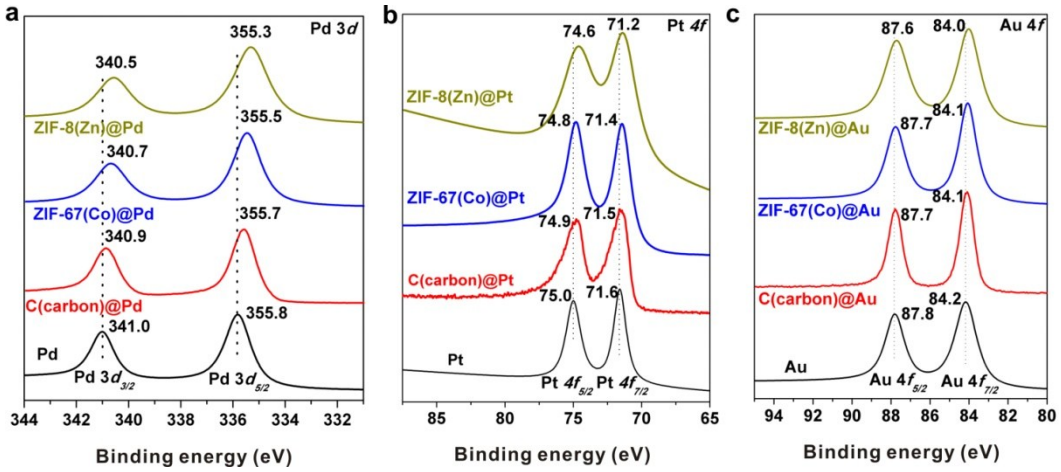


**Fig. S25** XPS profiles of different C(carbon)@M catalysts in respect with pure noble metal NPs, ZIF-67(Co)@M and ZIF-8(Zn)@M. (a) Pd 3*d* level, (b) Pt 4*f* level, and (c) Au 4*f* level. Numbers adjacent to dashed lines represent the binding energy values of the corresponding peaks.

It is evident that the interfacial interaction between ZIFs(Co/Zn) and noble metal NPs in both ZIF-67(Co)@M and ZIF-8(Zn)@M samples are stronger compared with that in C(carbon)@M samples (Table S1).

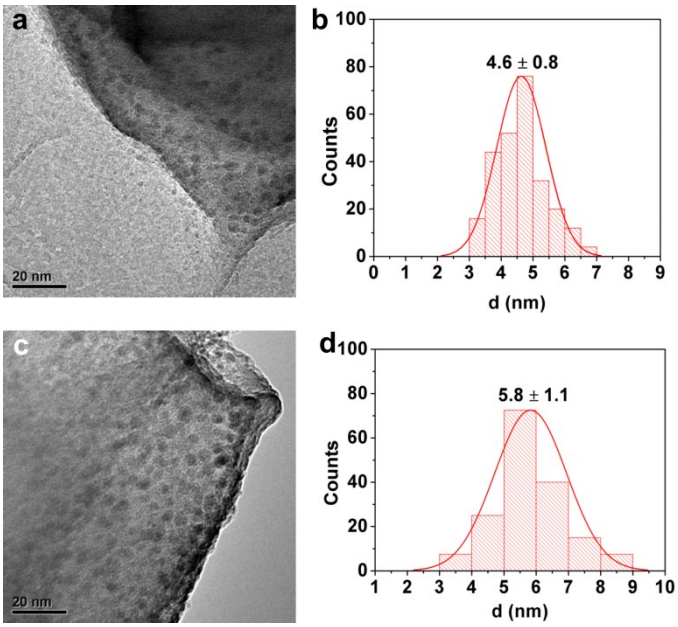


**Fig. S26** Morphology of ZIF-67(Co)@Pd sample and corresponding size histogram of Pd NPs. (a) TEM image of ZIF-67(Co)@Pd sample obained under the condition of 20 mg ZIF-67(Co), 300 μL $H_2PdCl_4$ aqueous solution (50 mM), and 1 mL methanol containing 15 mg $NaBH_4$, and (b) corresponding size histogram of Pd NPs. (c) TEM image of ZIF-67(Co)@Pd sample obained under the condition of 20 mg ZIF-67(Co), 300 μL $H_2PdCl_4$ aqueous solution (50 mM), and 1 mL methanol containing 20 mg $NaBH_4$, and (d) corresponding size histogram of Pd NPs.

ZIF-67(Co)@Pd samples characteristic with larger Pd NPs of 4.6 nm and 5.8 nm in diameter are obtained (Fig. S26), respectively, when the concentrations of reducing agent $NaBH_4$ are 15 and 20 $mg/mL_{methanol}$.

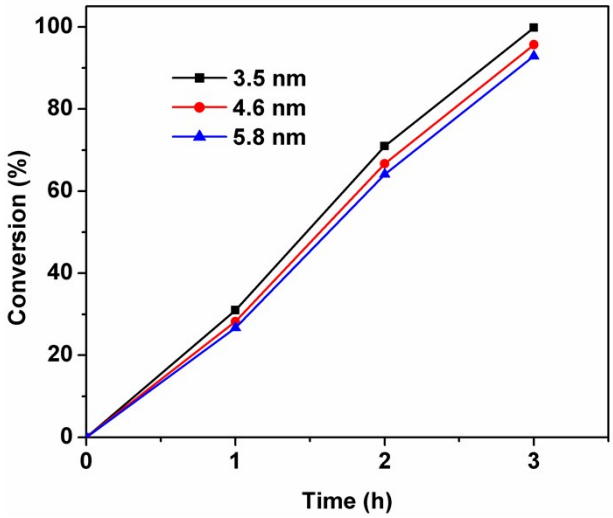


**Fig. S27** Catalytic liquid-phase benzaldehyde oxidation at the reaction temperature of 25 °C over ZIF-67(Co)@Pd samples with Pd NP sizes of ~3.5 nm, ~4.6 nm and ~5.8 nm, respectively.

When used as the catalysts for liquid-phase $C_6H_5CHO$ oxidation, the decrease in the catalytic activity is observed with increasing the average size of Pd in the ZIF-67(Co)@Pd samples, and correspondingly, the conversion rates are 99.8%, 95.7% and 92.9% at the reaction time of 3 h, respecively, when the Pd sizes are ~3.5, ~4.6 and ~5.8 nm in the ZIF-67(Co)@Pd samples.

**Table S1.** XPS analyses of Pd 3*d* level, Pt 4*f* level, and Au 4*f* level for different samples[a]

| Samples | Peak for $3d_{5/2}$ (eV) | Peak for $4f_{7/2}$ (eV) | Peak shift[b] (eV) |
|---|---|---|---|
| Pure Pd NP | 335.8 | – | – |
| ZIF-67(Co)@Pd | 335.5 | – | -0.3 |
| ZIF-8(Zn)@Pd | 335.3 | – | -0.5 |
| Pure Pt NP | – | 71.6 | – |
| ZIF-67(Co)@Pt | – | 71.4 | -0.2 |
| ZIF-8(Zn)@Pt | – | 71.2 | -0.4 |
| Pure Au NP | – | 84.2 | – |
| ZIF-67(Co)@Au | – | 84.1 | -0.1 |
| ZIF-8(Zn)@Au | – | 84.0 | -0.2 |
| C(Carbon)@Pd | 335.7 | – | -0.1 |
| C(Carbon)@Pt | – | 71.5 | -0.1 |
| C(Carbon)@Au | – | 84.1 | -0.1 |

[a] Peak position of different noble metal NPs including Pd, Pt and Au are obtained from XPS data shown in Figs 2, S13 and S25. [b] Peak shifts of different noble metal are calculated by comparing with pure noble metal NPs.

**Table S2.** Noble metal loading amount in different samples determined by ICP-MS, and the amount of each catalyst used in catalytic CO oxidation.

| Reaction | Samples | Noble metal size (nm) | Noble metal (wt.%) | Catalysts (mg) | Noble metal (mg) |
|---|---|---|---|---|---|
| CO oxidation | ZIF-67(Co)@Pd | 3.5 | 8.8 | 40 | 3.52 |
| | ZIF-67(Co)@Pt | 3.3 | 9.1 | 40 | 3.64 |
| | ZIF-67(Co)@Au | 3.3 | 8.6 | 40 | 3.44 |
| | ZIF-8(Zn)@Pd | 3.3 | 8.5 | 40 | 3.40 |
| | ZIF-8(Zn)@Pt | 3.3 | 8.7 | 40 | 3.48 |
| | ZIF-8(Zn)@Au | 3.4 | 8.9 | 40 | 3.56 |
| | C(carbon)@Pd | 3.0 | 10.9 | 32 | 3.52 |
| | C(carbon)@Pt | 4.0 | 6.3 | 56 | 3.54 |
| | C(carbon)@Au | 5.0 | 25.2 | 14 | 3.53 |
| $C_6H_5CHO$ oxidation | ZIF-67(Co)@Pd | 3.5 | 8.8 | 10 | 0.88 |
| | ZIF-67(Co)@Pt | 3.3 | 9.1 | 10 | 0.91 |
| | ZIF-67(Co)@Au | 3.3 | 8.6 | 10 | 0.86 |
| | ZIF-8(Zn)@Pd | 3.3 | 8.5 | 10 | 0.85 |
| | ZIF-8(Zn)@Pt | 3.3 | 8.7 | 10 | 0.87 |
| | ZIF-8(Zn)@Au | 3.4 | 8.9 | 10 | 0.89 |
| | C(carbon)@Pd | 3.0 | 10.9 | 8 | 0.87 |
| | C(carbon)@Pt | 4.0 | 6.3 | 14 | 0.87 |
| | C(carbon)@Au | 5.0 | 25.2 | 3.5 | 0.87 |
| | ZIF-67(Co)@Pd | 4.6 | 8.9 | 10 | 0.89 |
| | ZIF-67(Co)@Pd | 5.8 | 9.0 | 10 | 0.90 |

**Table S3.** Performance comparison of different catalysts towards CO oxidation.

| Catalyst | Size of NPs (nm) | GHSV (mL $h^{-1}g^{-1}_{cat}$) | $T_{100\%}$ ($^oC$) | Refs. |
|---|---|---|---|---|
| MIL-101(Cr)@Pt | 1.8 | 20000 | 175 | 14 |
| UiO-66(Zr)@Au | 2.8 | 15000 | 225 | 15 |
| Pt/UiO-66(Zr) | 3 | 19200 | 180 | 16 |
| Au@ZIF-8(Zn) | 4.2 | 60000 | 230 | 17 |
| Pt/ZIF-8(Zn) | 2.4 | 19200 | 190 | 18 |
| **ZIF-67(Co)@Pd** | **3.5** | **86250** | **120** | **This work** |

**Table S4.** Bader charge transfer (in e) from ZIFs to M(111) surfaces in ZIFs(Co/Zn)@M samples.

| | Pd(111) | Pt(111) | Au(111) |
|---|---|---|---|
| ZIF-67(Co) | -0.29 | -0.45 | -0.38 |
| ZIF-8(Zn) | -0.43 | -0.56 | -0.45 |

To understand the catalytic behaviour of CO oxidation, density functional theory (DFT) calculation was carried out using Vienna ab initio simulation package (VASP) with plane-wave pseudo potential method (Fig. S17). The result indicates that the most stable adsorption structure is that two N atoms from one ZIFs(Co/Zn) unit interact with M(111) surface to form N-M bonds with the length of ~2.1 Å (Fig. 4). After absorption on ZIFs(Co/Zn), M (111) surfaces are with negative charge, because the Lewis basic N of imidazole could act as electron donors (Table S4). Furthermore, more electrons are transferred from ZIF-8(Zn) to noble metal NPs compared with ZIF-67(Co)@M.

**Table S5.** Adsorption energy ($E_{ads}$, in eV) of CO on M(111) surface in ZIFs(Co/Zn)@M samples.

| | Pd | Pd-Co | Pd-Zn | Pt | Pt-Co | Pt-Zn | Au | Au-Co | Au-Zn |
|---|---|---|---|---|---|---|---|---|---|
| M(111) | -2.04 | -2.16 | -2.19 | -1.03 | -1.33 | -1.36 | -0.21 | -0.38 | -0.34 |

To understand the influence of electron transfer on CO adsorption, DFT simulation was performed to calculate the adsorption energy of CO on M(111) plane. Obviously, the adsorption energy of CO on M(111) plane in ZIF(Co/Zn)@M composites is increased compared with pure noble metals, due to the electron transfer from ZIFs to noble metal NPs (Table S5). Furthermore, the order of adsorption energy of CO on M(111) plane is Pd > Pt > Au, indicating that the enhanced catalytic activity of ZIF-67(Co)@Pd and ZIF-8(Zn)@Pd correlates with the interfacial interaction of noble metal NPs with ZIFs(Co/Zn).

**Table S6.** The *d*-band centers (in eV) of individual metal element in ZIFs(Co/Zn)@M samples compared with pure noble metal NPs.

| | Pd | Pd-Co | Pd-Zn | Pt | Pt-Co | Pt-Zn | Au | Au-Co | Au-Zn |
|---|---|---|---|---|---|---|---|---|---|
| M(d) | -1.43 | -1.50 | -1.52 | -1.70 | -1.82 | -1.91 | -3.22 | -2.91 | -2.91 |
| Co/Zn(d) | - | -1.68 | -6.91 | - | -1.55 | -6.79 | - | -1.86 | -6.66 |

As for M(111), the electron transfer has a slightly negative influence on the *d*-band center of M(111) (Table S6), for instance, the energy of *d*-bond center of Pd(111) is -1.43 eV for pure Pd, -1.50 eV for ZIF-67(Co)@Pd and -1.52 eV for ZIF-8(Zn)@Pd. In regard of the *d*-band center of Co or Zn in ZIFs(Co/Zn), the energy of *d*-band center of Co is -1.68 eV for ZIF-67(Co)@Pd, -1.55 eV for ZIF-67(Co)@Pt and -1.86 eV for ZIF-67(Co)@Au, while the energy for *d*-band center of Zn is -6.91 eV for ZIF-8(Zn)@Pd, -6.79 eV for ZIF-8(Zn)@Pt and -6.66 eV for ZIF-8(Zn)@Au. It is interesting to be noted that the energy of the *d*-band center of M(111) and Co is -1.50 *vs.* -1.68 eV for ZIF-67(Co)@Pd, -1.82 *vs.* -1.55 eV for ZIF-67(Co)@Pt, and -2.91 *vs.* -1.86 eV for ZIF-67(Co)@Au. Among them, the *d*-band center of Pd(111) and Co in ZIF-67(Co)@Pd is more closer to the Fermi level, thus leading to the highest catalytic activity (Fig. 3a and b).

**Table S7.** Catalytic oxidation of benzaldehyde at the reaction time of 5 h by different catalysts

| Catalysts | Conversion of benzaldehyde (%) |
|---|---|
| Blank | 9.7 |
| ZIF-67(Co) | 11.9 |
| ZIF-8(Zn) | 10.2 |

It is noticed that without catalyst, the conversion rate of benzaldehyde is around 9.7% without catalyst. At the same reaction conditions, the conversion rate is about 11.9% for ZIF-67(Co), while as for ZIF-8(Zn), the conversion rate is about 10.2%. Therefore, ZIFs themselves have almost no activity (less than 2.2%) for oxidation of benzaldehyde.

**References**

[1] H. Y. Li, H. Ma, X. H. Wang, J. Gao, C. Chen, S. Shi, M. J. Qu, N. Feng and J. Xu, *J. Energy Chem.*, 2014, **23**, 742–746.

[2] N. L. Torad, M. Hu, Y. Kamachi, K. Takai, M. Imura, M. Naito and Y. Yamauchi, *Chem. Commun.*, 2013, **49**, 2521–2523.

[3] K. Leus, P. Concepcion, M. Vandichel, M. Meledina, A. Grirrane, D. Esquivel, S. Turner, D. Poelman, M. Waroquier, V. Van Speybroeck, G. Van Tendeloo, H. García and P. Van Der Voort, *RSC Adv.*, 2015, **5**, 22334–22342.

[4] G. Kresse and J. Hafner, *Phys. Rev. B*, 1993, **47**, 558–561.

[5] G. Kresse and J. Furthmuller, *Phys. Rev. B*, 1996, **54**, 11169–11186.

[6] J. P. Perdew, K. Burke and M. Ernzerhof, *Phys. Rev. Lett.*, 1996, **77**, 3865–3868.

[7] P. E. Blöchl, *Phys. Rev. B*, 1994, **50**, 17953–17979.

[8] G. Kresse and D. Joubert, *Phys. Rev. B*, 1999, **59**, 1758–1775.

[9] H. C. Li, W. J. Liu, H. X. Han and H. Q. Yu, *J. Mater. Chem. A*, 2016, **4**, 11680–11687.

[10] T. Jiang, D. J. Mowbray, S. Dobrin, H. Falsig, B. Hvolbaek, T. Bligaard and J. K. Norskov, *J. Phys. Chem. C*, 2009, 113, 10548–10553.

[11] Y. Lykhach, S. M. Kozlov, T. Skala, A. Tovt, V. Stetsovych, N. Tsud, F. Dvorak, V. Johanek, A. Neitzel, J. Myslivecek, S. Fabris, V. Matolin, K. M. Neyman and J. Libuda, *Nat. Mater.*, 2016, **15**, 284–288.

[12] D. S. Choi, A. W. Robertson, J. H. Warner, S. O. Kim and H. Kim, *Adv. Mater.*, 2016, **28**, 7115–7122.

[13] V. Stamenkovic, B. S. Mun, K. J. J. Mayrhofer, P. N. Ross, N. M. Markovic, J. Rossmeisl, J. Greeley and J. K. Norskov, *Angew. Chem. Int. Ed.*, 2006, **118**, 2963–2967.

[14] A. Aijaz, T. Akita, N. Tsumori and Q. Xu, *J. Am. Chem. Soc.*, 2013, **135**, 16356–16359.

[15] R. B. Wu, X. K. Qian, K. Zhou, H. Liu, B. Yadian, J. Wei, H. W. Zhu and Y. Z. Huang, *J. Mater. Chem. A*, 2013, **1**, 14294–14299.

[16] W. Zhang, G. Lu, C. Cui, Y. Liu, S. Li, W. Yan, C. Xing, Y. R. Chi, Y. Yang and F. Huo, *Adv. Mater.*, 2014, **26**, 4056–4060.

[17] H. L. Jiang, B. Liu, T. Akita, M. Haruta, H. Sakurai and Q. Xu, *J. Am. Chem. Soc.*, 2009, **131**, 11302–11303.

[18] G. Lu, S. Z. Li, Z. Guo, O. K. Farha, B. G. Hauser, X. Y. Qi, Y. Wang, X. Wang, S. Y. Han, X. G. Liu, J. S. DuChene, H. Zhang, Q. C. Zhang, X. D. Chen, J. Ma, S. C. J. Loo, W. D. Wei, Y. H. Yang, J. T. Hupp and F. W. Huo, *Nat. Chem.*, 2012, **4**, 310–316.